A General Approach to Porous Crystalline TiO_2, $SrTiO_3$, and $BaTiO_3$ Spheres

Yawen Wang,[†] Hua Xu,[†] Xiaobing Wang,[†] Xi Zhang,[†] Huimin Jia,[†] Lizhi Zhang,*[,†] and Jianrong Qiu[‡]

Key Laboratory of Pesticide & Chemical Biology, Ministry of Education, College of Chemistry, Central China Normal University, Wuhan, 430079, People's Republic of China, and National Coal Combustion Laboratory, Huazhong University of Science and Technology, Wuhan, 430074, People's Republic of China

Received: March 14, 2006; In Final Form: May 22, 2006

Monodispersed porous crystalline TiO_2, $SrTiO_3$, and $BaTiO_3$ spheres were produced through a one-step hydrothermal process from amorphous TiO_2 spheres. The resulting samples were characterized by scanning electron microscopy (SEM), transmission electron microscopy (TEM), X-ray diffraction (XRD), and nitrogen sorption measurements. On the basis of the characterization results, we proposed a formation process of these porous spheres according to a mechanism analogous to the Kirkendall effect. This study provides a general way to synthesize porous titania-based spheres.

1. Introduction

Titanium dioxide (TiO_2) and perovskite-type materials of ABO_3, such as strontium titanate ($SrTiO_3$) and barium titanate ($BaTiO_3$), are widely used in modern electronic devices. Since the discovery of photoinduced water splitting on titanium dioxide electrodes in 1972,[1] TiO_2 has been intensively investigated as photocatalysts in the fields of solar energy conversion, water splitting, and environmental purification.[2−8] Besides, TiO_2 is also the most used pigment in paintings and textiles.[9] $SrTiO_3$ and $BaTiO_3$ have often been used in the preparation of dense ferroelectrics, thin-film electronic components, and electric-optical materials; for instance, strontium titanate has applications as a dielectric and photoelectric material while barium titanate is the main dielectric material component of class II ceramic capacitors.[10]

Since mesoporous TiO_2 was first synthesized through modified sol−gel routes in the presence of alklyphosphate surfactant templates by Antonelli and Ying in 1995,[11] many different routes about the synthesis of mesoporous TiO_2 spheres have been reported constantly. They include sonochemical approach,[12,13] aerosol technique,[14] hydrothermal method,[15] microwave hydrothermal technology,[16] and so on, while $SrTiO_3$ and $BaTiO_3$ are traditionally prepared by solid-state reaction,[17,18] oxalic coprecipitate method,[19,20] sol−gel technique,[21,22] and hydrothermal method.[23−25] In recent years, there were some new methods to fabricate porous $SrTiO_3$. These methods include the sonochemical method to prepare size-tunable strontium titanate crystals reported by us[26] and the inverse micelle microemulsion method to fabricate $SrTiO_3$ nanopowders, a method by Li and Lai.[27]

However, there is not a general method to synthesize porous crystalline TiO_2, $SrTiO_3$, and $BaTiO_3$ spheres. In this study, we report that monodispered porous crystalline TiO_2, $SrTiO_3$, and $BaTiO_3$ spheres can be prepared by a general hydrothermal method. On the basis of the characterization results, the formation processes of the porous spheres are proposed according to a mechanism analogous to the Kirkendall effect.

* To whom correspondence should be addressed. E-mail: zhanglz@mail.ccnu.edu.cn. Tel/Fax: +86-27-6786 7535.

[†] Central China Normal University.

[‡] Huazhong University of Science and Technology.

2. Experimental Section

2.1. Preparation of Monodispersed Amorphous Spherical TiO_2 Particles. All chemicals were used as received. Monodispersed amorphous spherical TiO_2 particles were prepared by controlled hydrolysis of titanium tetraisopropoxide (TTIP, $Ti(OC_3H_7)_4$, 97%, Aldrich) in ethanol.[28] Typically, 100 mL of ethanol was mixed with 0.4 mL of 0.1 M aqueous potassium chloride, followed by the addition of 2.2 mL of TTIP at ambient temperature. The solution was mixed completely using a magnetic stirrer for about 10 min until a white precipitate appeared. The suspension was aged in a static condition for 24 h in a closed container at room temperature in air atmosphere. The powder (denoted as AT) deposited at the bottom of the vessel was collected and dried at 50 °C in air.

2.2. Preparation of Crystalline TiO_2. An amount of 0.2 g of AT was added to 15 mL of distilled water. The resulting suspension was transferred into a 20 mL Teflon-lined stainless steel autoclave and then placed in an oven at 180 °C for 12 h. The powder (denoted as CT) was collected by filtration, washed with ethanol thoroughly, and finally dried in an oven at 50 °C.

2.3. Preparation of Crystalline $SrTiO_3$ and $BaTiO_3$. The preparation of porous $SrTiO_3$ and $BaTiO_3$ is as follows: AT and strontium (barium) hydroxide hydrates were added with an equivalent molar ratio of Sr (Ba)/Ti in 15 mL of distilled water. The suspension was transferred into a 20 mL Teflon-lined stainless steel autoclave and then placed in an oven at 180 °C for 12 h. The resulting white powders (denoted as ST or BT) were collected by filtration, then washed with a 1.0 M aqueous acetic acid solution and ethanol thoroughly, and finally dried in an oven at 50 °C.

2.4. Characterization. X-ray powder diffraction (XRD) patterns were obtained using a Philips MPD 18801 diffractometer using Cu Kα radiation. Scanning electron microscopy (SEM) measurements were performed used a JSM-5600 SEM. Transmission electron microscopy (TEM) study and energy-dispersive X-ray spectra (EDS) were carried out on a Philips CM-120 electron microscopy instrument. The samples for TEM were prepared by dispersing the final powders in ethanol; the dispersion was then dropped on carbon−copper grids. The nitrogen adsorption and desorption isotherms at 77 K were

10.1021/jp061597t CCC: $33.50
Published on Web 06/27/2006

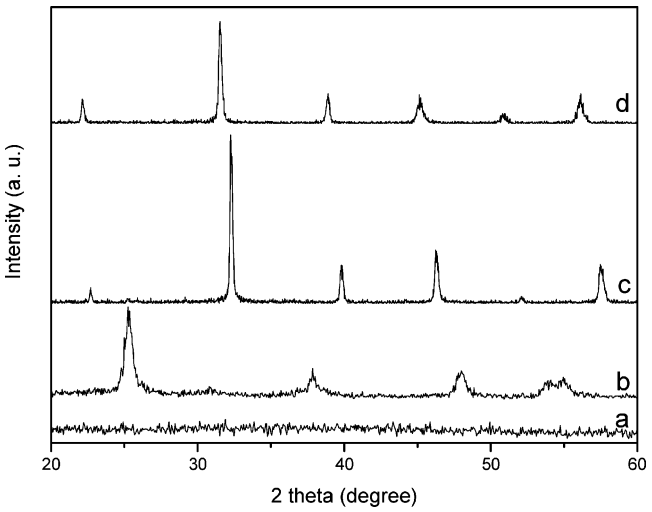

Figure 1. XRD patterns of (a) sample AT, (b) sample CT, (c) sample ST, and (d) sample BT.

measured using a Micrometrics ASAP2010 system after the samples were vacuum-dried at 200 °C overnight.

3. Results and Discussion

3.1. XRD Patterns. Figure 1 shows the X-ray diffraction (XRD) patterns of AT and the samples prepared hydrothermally from AT. No diffraction peaks in the XRD pattern of AT were found (Figure 1a), indicating the amorphous nature of the sample obtained by hydrolysis of TTIP. From XRD measurements, it is seen that the XRD data of CT match the standard anatase pattern (JCPDS No. 21-1272) (Figure 1b). This result reveals that CT prepared from amorphous TiO_2 by the hydrothermal method is pure anatase. The XRD patterns of ST and BT (Figure 1c, 1d) can well be indexed to cubic strontium titanate (JCPDS No. 73-0661) and barium titanate (JCPDS No. 74-1968), respectively. There is no difference between the patterns of ST and BT except for a shift of Bragg angle. This shifting is considered to be caused by the difference in ionic radii of Ba^{2+} and Sr^{2+}. From the XRD results, we conclude that crystalline TiO_2, $SrTiO_3$, and $BaTiO_3$ can be obtained through a one-step hydrothermal reaction from amorphous TiO_2.

3.2. SEM Images. The morphologies of the resulting samples were investigated by scanning electron microscopy. Figure 2 shows the SEM images of amorphous titania, crystalline TiO_2, $SrTiO_3$, and $BaTiO_3$. From Figure 2a, we found that the amorphous titania consisted of well-defined spheres with sizes of 300 to 500 nm. The surfaces of these spheres were relatively smooth. After crystallization, the sizes of these spheres kept unchanged. However, their surfaces became rough (Figure 2b). Obviously, the spheres of crystalline TiO_2 were composed of small monodispersed primary particles of several nanometers in size. Macropores or large mesopores formed among the big secondary spheres, and the mesopores among the small primary particles produced a hierarchical porous structure in crystalline TiO_2. After the amorphous TiO_2 spheres reacted with $Sr(OH)_2$, monodisphersed spheres with about 400 nm in size were obtained in the resulting $SrTiO_3$ (Figure 3c). These $SrTiO_3$ spheres also consisted of small monodispersed primary particles of about 20 nm in size, which were larger than those in the crystalline TiO_2 spheres. Therefore, a hierarchical porous structure also existed in $SrTiO_3$. Interestingly, some semispheres were found in $SrTiO_3$. They were believed to be broken by the

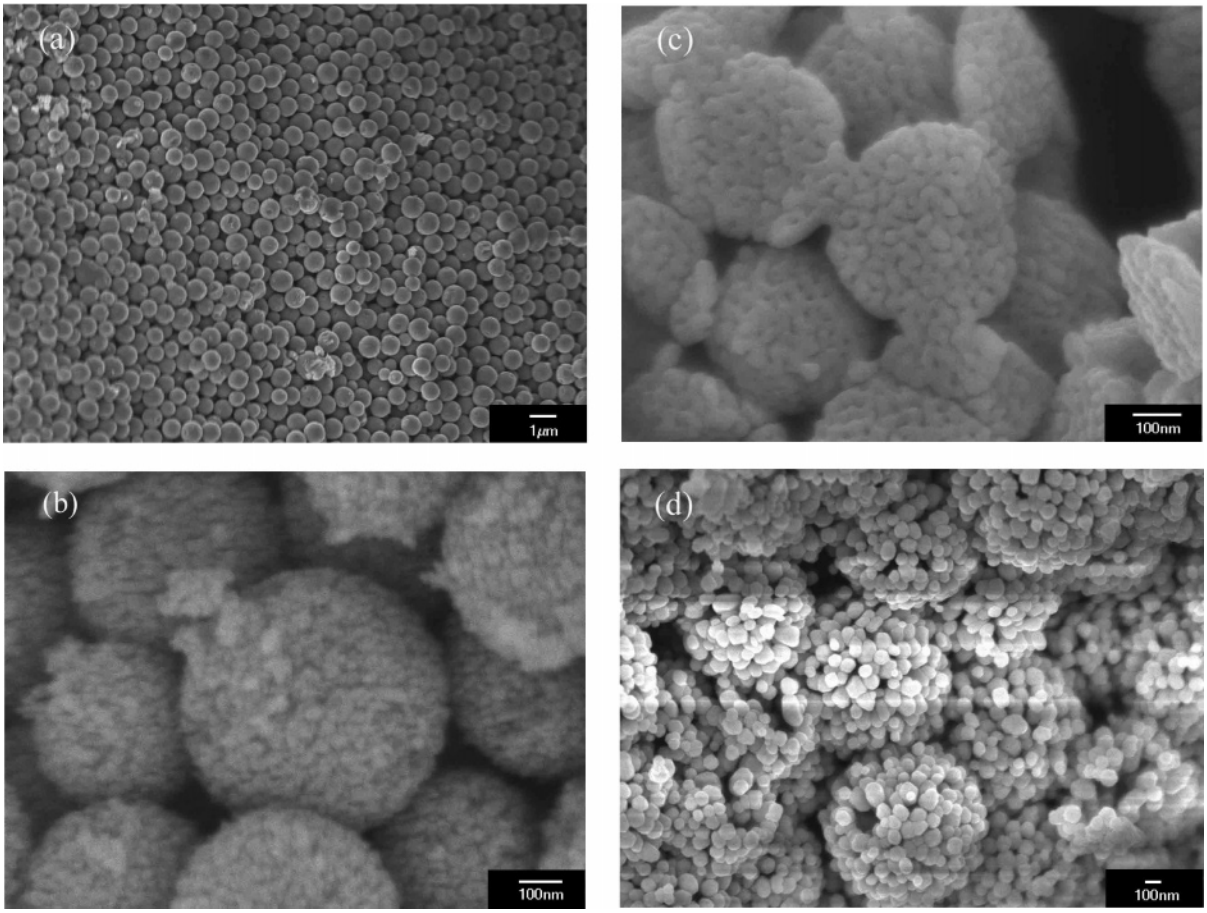

Figure 2. SEM images of (a) AT, (b) CT, (c) ST, and (d) BT.

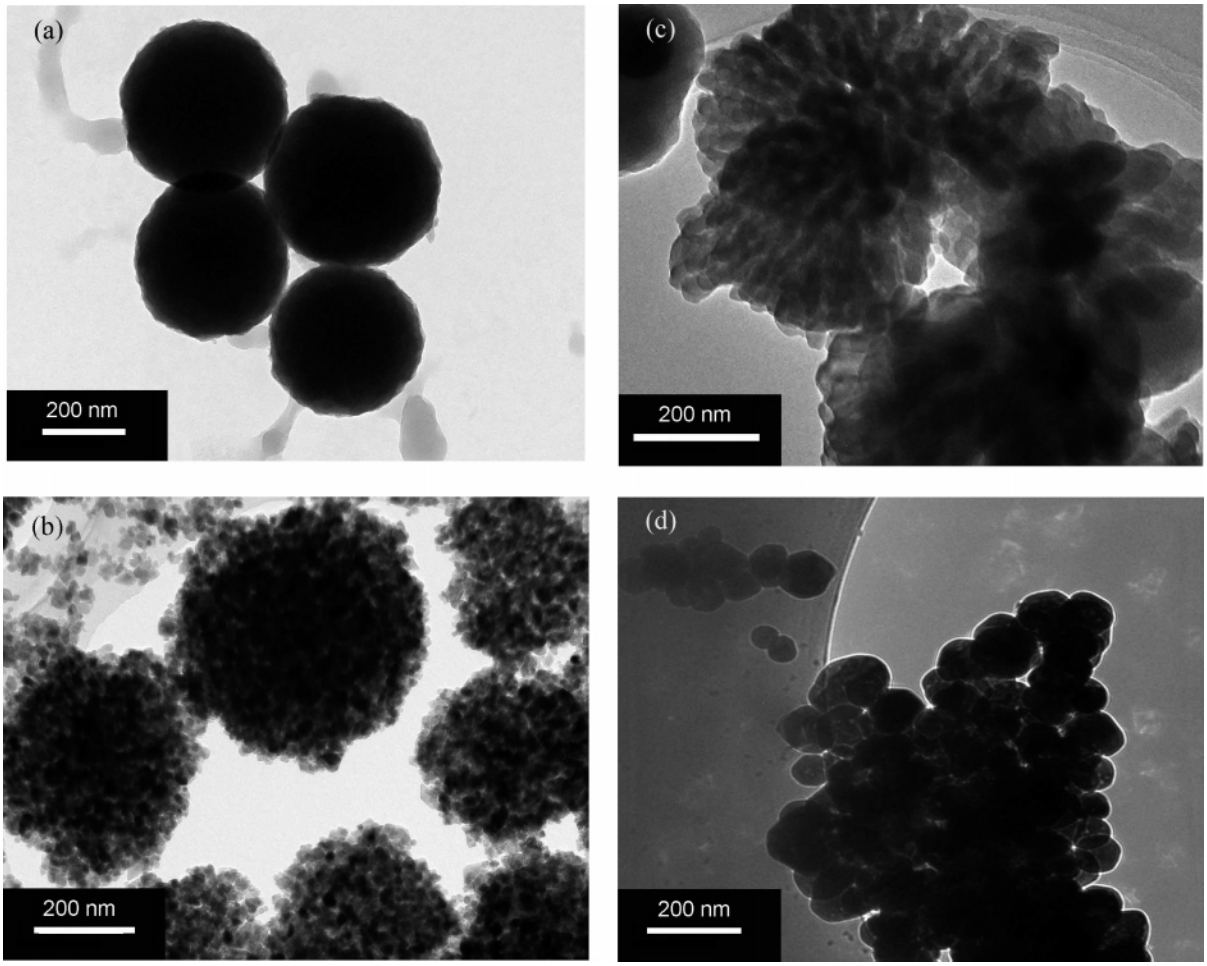

Figure 3. TEM images of (a) AT, (b) CT, (c) ST, and (d) BT.

hydrothermal process. The morphology of $BaTiO_3$ is different from those of crystalline TiO_2 and $SrTiO_3$. Big spheres of several hundreds nanometers in size were still visible (Figure 3d). However, the connections among the small primary particles in the big spheres of $BaTiO_3$ were not as tight as those of crystalline TiO_2 and $SrTiO_3$ (Supporting Information). These small particles were of about 100 nanometers, significantly larger than those of crystalline TiO_2 and $SrTiO_3$ primary particles. These differences may be related to the different reaction rates, which will be discussed later.

3.3. TEM Images. The microstructures of the samples were further investigated by transmission electron microscopy. Figure 3a shows the TEM image of amorphous TiO_2. It was found that some well-defined spheres of about 400 nm in sizes were connected to each other to form pores in the range of 50 to 100 nm. During the sonication for TEM measurement, some small primary particles were dropped from the big spheres of CT (Figure 3b). These monodispersed primary particles are of about 10 nm in size, in agreement with SEM observation. Most of the big secondary spheres in CT were still preserved well after sonication. These secondary spheres are slightly larger than those of amorphous titania. Mesopores formed among the small primary particles in the big spheres of CT, while macropores or large mesopores produced among the big secondary spheres of CT were also observed. This confirms the existence of a hierarchical porous structure in CT. The TEM image of $SrTiO_3$ is similar to that of crystalline TiO_2 except that the sizes of the primary particles in the big spheres are larger than that of crystalline TiO_2 (Figure 3c). This is consistent with the XRD and SEM results. Because of the large sizes and loose connections of the small particles in $BaTiO_3$, well-defined spheres were difficult to find in the TEM image of $BaTiO_3$ after sonication. If the sample for TEM measurement was not prepared by sonication, we could observe mesopores in the TEM image (Figure 3d). Part of the small particles still "glued" together, producing these mesopores among the spherical particles.

3.4. Nitrogen Sorption. The porous structures of the resulting samples were studied by nitrogen sorption. Figure 4 presents the nitrogen adsorption−desorption isotherms and Barret−Joyner−Halenda (BJH) pore size distribution curves (inset) of the samples. Figure 4a exhibits a Type I adsorption−desorption isotherm, which is typically characteristic of microporous materials having relatively small external surfaces.[29] In the nitrogen adsorption−desorption isotherms of AT, there is a hysteresis loop at $0.92 < P/P_0 < 0.98$, corresponding to the filling of larger textural mesopores produced by interaggregated secondary particles. This confirms the TEM result of Figure 2a. Therefore, we conclude that amorphous TiO_2 possesses a hierarchical porous structure (micro- and mesopores). Two distinct capillary condensation steps can clearly be seen in the nitrogen adsorption−desorption isotherms of crystalline TiO_2 (Figure 4b). These confirm the hierarchical porous system of crystalline TiO_2. The first hysteresis loop of crystalline TiO_2 is at $0.7 < P/P_0 < 0.95$, corresponding to the filling of the framework confined mesopores formed between intra-agglomerated primary particles. The second hysteresis loop is at $0.95 < P/P_0 < 1$, corresponding to the filling of textural meso- and macropores produced by interaggregated secondary par-

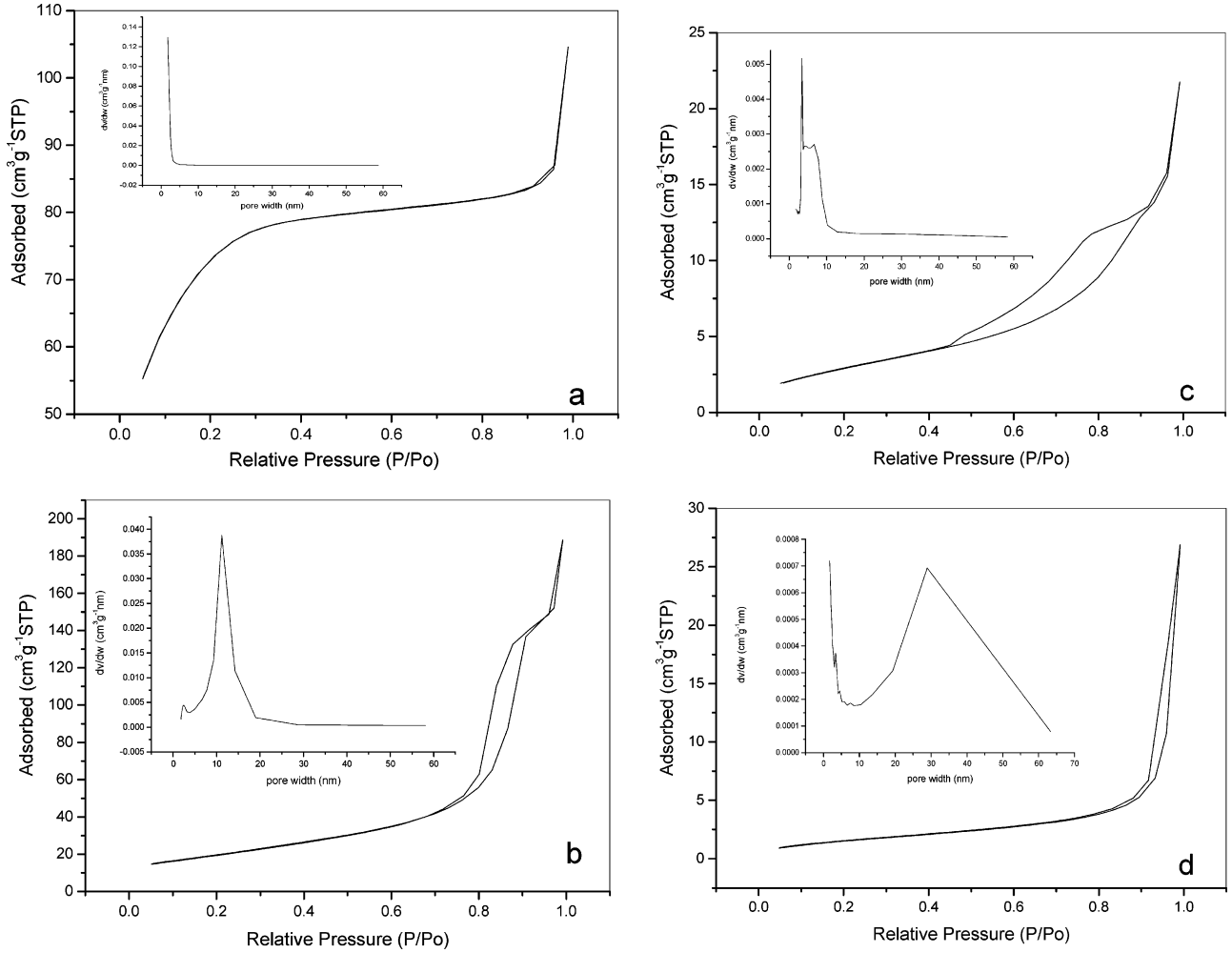

Figure 4. Nitrogen adsorption−desorption isotherm and pore size distribution curve (inset) of (a) AT, (b) CT, (c) ST, and (d) BT.

TABLE 1: Textural Properties of AT, CT, ST, and BT

sample	A_{BET} (m^2/g)	V_{BJH} (cm^3/g)	pore diameter (nm)
amorphous TiO_2	245.6	0.12	3.0
crystalline TiO_2	128.5	0.45	11.3, 2.1
$SrTiO_3$	11.2	0.03	6.6
$BaTiO_3$	11.4	0.08	29.7

ticles. Differently, there is only a single hysteresis loop in the nitrogen adsorption−desorption isotherms of $SrTiO_3$ and $BaTiO_3$, respectively. This may be because of small percentages of these textural meso- and macropores in all the pores of $SrTiO_3$ and $BaTiO_3$. The Brunauer−Emmett−Teller (BET) specific surface areas, pore volumes, and mean pore diameters of amorphous TiO_2, crystalline TiO_2, $SrTiO_3$, and $BaTiO_3$ are summarized in Table 1.

3.5. Formation Processes of the Porous Structures in Crystalline TiO_2, $SrTiO_3$, and $BaTiO_3$. A dissolution−crystallization mechanism has been used to illustrate the nucleation and growth procedures of $SrTiO_3$ and $BaTiO_3$ on Ti-metal substrates and Ti-metal substrates and Ti-coated substrate prepared by hydrothermal or hydrothermal-electrochemical methods.[30,31] We believe that the crystallization of $SrTiO_3$ and $BaTiO_3$ can also be explained by the dissolution−crystallization mechanism, which was discussed extensively before. So in this study we want to focus on the formation processes of the porous structures of CT, ST, and BT.

In our previous works, a hierarchical porous titania was thought to be produced through the interaggregation (or interagglomeration) of mesoporous titania spheres under sonication.[12] Recently, we fabricated hierarchical porous iron oxide films on iron metal foils. The formations of these hierarchical porous films were explained by a mechanism analogous to the Kirkendall effect.[32] In this paper, we think that the porous structure formations of crystalline TiO_2, $BaTiO_3$, and $SrTiO_3$ can also be explained by a mechanism analogous to the Kirkendall effect. Their common formation processes might be represented in Scheme 1.

SCHEME 1: Illustration of the Possible Formation Mechanism of Porous Crystalline TiO_2, $BaTiO_3$, and $SrTiO_3$

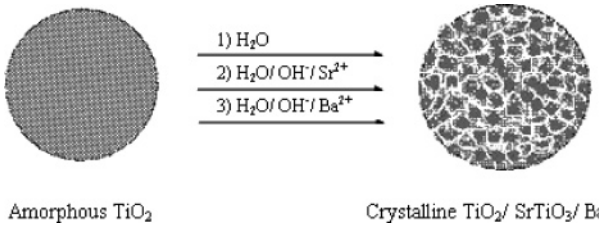

In 1947, Kirkendall reported the movement of the interface between a diffusion couple, that is, copper and zinc in brass, as the result of the different diffusion rates of these two species at an elevated temperature.[33] This phenomenon, now called the Kirkendall effect, was the first experimental proof that atomic diffusion occurs through vacancy exchange and not by the direct interchange of atoms. The net directional flow of matter is

balanced by an opposite flow of vacancies, which can condense into pores or annihilate at dislocations. A common result from this effect is the formation of porosity in the lower-melting component side of the diffusion couple.[34] The pore formation during the growth of metal oxide films can be explained by the fast outward diffusion of cations through the oxide layer accompanied by an inward flow of vacancies to the vicinity of the metal-oxide interface.[35]

The formation of hierarchical porous structure of crystalline TiO_2 formation can be explained as follows. Because the amorphous TiO_2 spheres had microporous structure, water molecules first entered the spheres and interacted with Ti−OH groups to form $Ti-OH_2^+$.[36] These protonated Ti−OH groups easily combined with −OH groups of other TiO_6 octahedra to form Ti−O−Ti oxygen bridge bonds by eliminating a water molecule.[37] This process led to the outward flow of $Ti-OH_2^+$ formed in reaction through the shell which resulted in supersaturation of vacancies. Then annihilation of excess vacancies at dislocations and boundaries produced stresses that led to the formation of cracks near the interface; the cracks then acted as nuclei for the further condensation of supersaturated vacancies. Finally, mesoporous could be formed in the spheres by outward transport of fast-moving $Ti-OH_2^+$ through the oxide layer and a balancing inward flow of vacancies to the vicinity of the surfaces of TiO_2 spheres. These resulting mesopores formed between intra-agglomerated primary particles and the large mesopores produced by interaggregated secondary spheres consisted of the hierarchical porous structure of CT, as revealed in Figure 4b.

After amorphous titania were added to $Sr(OH)_2$ or $Ba(OH)_2$ solution, OH^- and H_2O would enter into the amorphous titania spheres and interact with the titanium ions and/or lattice oxygen to form titanium hydroxyl species (probably $HTiO_3^-$).[38] Then, $HTiO_3^-$ reacted with Sr^{2+} or Ba^{2+} ions to form $SrTiO_3$ or $BaTiO_3$ particles, where the diffusion of $HTiO_3^-$ through the shell was balanced by the opposite flow of vacancies to the vicinity of the TiO_2 surfaces. Different from the formation process of porous crystalline TiO_2, the presence of abundant OH^- would promote the fast formation of $HTiO_3^-$. The subsequent fast diffusing $HTiO_3^-$ ions drove the vacancy injection to increase too quickly,[35] which caused the partial or complete collapse of the porous structures formed between intra-agglomerated primary particles in $SrTiO_3$ and $BaTiO_3$. This is the reason for the existence of a single hysteresis loop in the nitrogen adsorption−desorption isotherms of $SrTiO_3$ and $BaTiO_3$. Because the alkalinity of the $Ba(OH)_2$ solution was stronger than that of the $Sr(OH)_2$ solution, resulting in higher vacancy injection, the collapse extent of the porous structure in $BaTiO_3$ is worse than that in $SrTiO_3$. This result further confirms our proposed formation processes of these porous spheres.

4. Conclusions

In this study, we developed a general approach to fabricate porous crystalline TiO_2, $SrTiO_3$, and $BaTiO_3$ spheres. This route consists of two steps: (1) precipitation of amorphous TiO_2 spheres and (2) hydrothermal conversion of the amorphous TiO_2 spheres into porous crystalline TiO_2, $SrTiO_3$, and $BaTiO_3$ spheres. The formation of porous structures of these crystalline TiO_2, $SrTiO_3$, and $BaTiO_3$ spheres could be explained by a mechanism analogous to the Kirkendall effect; that is, the porous was formed by outward transport of fast-moving $Ti-OH_2^+$ or $HTiO_3^-$ through the oxide layer and a balancing inward flow of vacancies to the vicinity of the TiO_2 interface. This study provides a general way to synthesize porous titania-based spheres. These resulting porous spheres may find applications in the fields of catalysis, ferroelectrics, photoelectrics, and so forth.

Acknowledgment. The work described in this paper was partially supported by National Science Foundation of China (Grant 20503009), Outstanding Young Research Award of National Natural Science Foundation of China (Grant 50525619), and Open Fund of Key Laboratory of Catalysis and Materials Science of Hubei Province (Grant CHCL0508).

Supporting Information Available: XRD patterns of $SrTiO_3$ and $BaTiO_3$ without acid-rinsing; high-magnification SEM image of amorphous TiO_2; SEM images of amorphous TiO_2, crystalline TiO_2, $SrTiO_3$ and $BaTiO_3$; EDX spectrums of $SrTiO_3$ and $BaTiO_3$. This material is available free of charge via the Internet at http://pubs.acs.org.

References and Notes

(1) Fujishima, A.; Honda, K. *Natrue* **1972**, *37*, 238.
(2) Hoffmann, M. R.; Martin, S. T.; Choi, W.; Bahnemann, K. W. *Chem. Rev.* **1995**, *95*, 96.
(3) Linsebigler, L.; Lu, G.; Yates, T. J. *Chem. Rev.* **1995**, *95*, 735.
(4) Fox, M. A.; Dulay, M. T. *Chem. Rev.* **1993**, *93*, 341.
(5) Yoko, T.; Yuasa, A.; Kamia, K.; Sakka, S. *J. Electrochem. Soc.* **1991**, *138*, 2279.
(6) Hagfeldt, A.; Gratzel, M. *Chem. Rev.* **1995**, *95*, 49.
(7) Aurian-Blajeni, B.; Halman, M.; Manassen, J. *J. Solar Energy* **1980**, *25*, 165.
(8) Cristiani, C.; Belloto, M. L.; Forzatti, P. L.; Bregani, F. *J. Mater. Res.* **1993**, *8*, 2019.
(9) Anderson, S.; Collen, B.; Kuylenstierna, V.; Magnelli, A. *Acta Chem. Scand.* **1957**, *11*, 1641.
(10) Moreno, J.; Dominguez, J. M.; Montoya, A.; Vicente, L.; Viveros, T. *J. Mater. Chem.* **1995**, *5*, 509.
(11) Antonelli, D. M.; Ying, Y. J. *Angew. Chem., Int. Ed. Eng.* **1995**, *34*, 2014.
(12) Zhang, L. Z.; Yu, J. C. *Chem. Commun.* **2003**, 2078.
(13) Zhang, Y. X.; Li, G. H.; Wu, Y. C.; Luo, Y. Y.; Zhang, L. D. *J. Phys. Chem. B* **2005**, *109*, 5478.
(14) Huisman, C. L.; Goossens, A.; Schoonman, J. *Chem. Mater.* **2003**, *15*, 4617.
(15) Cho, C.; Han, M.; Kim, D. H.; Kim, D. K. *Mater. Chem. Phys.* **2005**, *92*, 104.
(16) Wilson, G. J.; Will, G. D.; Frost, R. L.; Montgomery, S. A. *J. Mater. Chem.* **2002**, *12*, 1787.
(17) Kononyuk, I. F.; Lomonosov, V. A.; Panasyugin, A. S.; Yushkevich, I. I.; Zonov, Y. G. *Key Eng. Mater.* **1997**, *117*, 132.
(18) Wold, A.; Dwight, K. *J. Solid State Chem.* **1990**, *88*, 229.
(19) Potdar, H. S.; Deshpande, S. B.; Godbole, P. D.; Gunjikar, V. G.; Date, S. K. *J. Mater. Res.* **1992**, *7*, 429.
(20) Guang, J.; Choi, S. K.; Kyoung, J.; Woo, L.; Kee, K. K. *Chem. Mater.* **1998**, *10*, 4104.
(21) Selvaraj, U.; Prasadarao, A. V.; Komarneni, S.; Roy, R. *Mater. Lett.* **1995**, *23*, 123.
(22) Bernadette, A.; Ki-Seog, C. *Chem. Mater.* **2002**, *14*, 480.
(23) Kumazawa, H.; Annen, S.; Sada, E. *J. Mater. Sci.* **1995**, *30*, 4740.
(24) Jing, Y.; Jin, S.; Jia, Y. Z.; Han, J. D.; Sun, J. H. *J. Mater. Sci.* **2005**, *40*, 6315.
(25) Xu, H. R.; Gao, L.; Guo, J. K. *J. Eur. Ceram. Soc.* **2002**, *22*, 1163.
(26) Yu, J. C.; Zhang, L. Z.; Li, Q.; Li, Q.; Kwong, K. W.; Xu, A. W.; Lin, J. *Langmuir* **2003**, *19*, 7673.
(27) Li, Y. F.; Lai, Q. Y. *Chin. J. Inorg. Chem.* **2005**, *21*, 915.
(28) Barringer, E. A.; Bowen, H. K. *Commun. Am. Ceram. Soc.* **1982**, *65*, 199.
(29) Sing, K. S. W.; Everett, D. H.; Haul, R. A. W.; Moscou, L.; Pierotti, R. A.; Rouquerol, J.; Siemieniewska, T. *Pure Appl. Chem.* **1985**, *57*, 603.
(30) Yoshimura, M.; Suchanek, W.; Han, K. S. *J. Mater. Chem.* **1999**, *9*, 77.
(31) Yoshimura, M.; Yoo, S. E.; Hayashi, M.; Ishizawa, N. J. *J. Appl. Phys.* **1989**, *28*, 2007.
(32) Zhang, L. Z.; Yu, J. C.; Zheng, Z.; Leung, C. W. *Chem. Commun.* **2005**, 2683.
(33) Smigelskas, A. D.; Kirkendall, E. O. *Trans. Aime.* **1947**, *130*, 171.
(34) Liu, B.; Zeng, H. C. *J. Am. Chem. Soc.* **2004**, *126*, 16744.

(35) Yin, Y. D.; Rioux, R. M.; Erdonmez, C. K.; Hughes, S.; Somorjai, C. A.; Alivisatos, A. P. *Science* **2004**, *304*, 711.

(36) Brinker, C. J.; Scherer, G. W. In *Sol−Gel Science: The Physics and Chemistry of Sol−Gel Processing*; Academic Press: New York, 1990, p 240.

(37) Yin, H.; Wada, Y.; Kitamura, T.; Kambe, S.; Murasawa, S.; Mori, H.; Sakata, T.; Yangaida, S. *J. Mater. Chem.* **2001**, *11*, 1694.

(38) Pourbaix, M. In *Atlas of Electrochemical Equilibria in Aqueous Solutions*, 2nd ed.; National Association of Corrosion/Engineers: Houston, TX, 1974; p 251.